Contract No:

This document was prepared in conjunction with work accomplished under Contract No. DE-AC09-08SR22470 with the U.S. Department of Energy.

Disclaimer:

SRNS-STI-2009-00425

Characterization of Secondary Phases in Modified Vertical Bridgman Growth CZT

Martine C. Duff*, *Savannah River National Laboratory, Aiken, SC 29808*

Kelvin G. Lynn, Kelly Jones *Washington State University, Pullman, WA*

Zurong R. Dai, John P. Bradley, Nick Teslich, *Lawrence Livermore National Laboratory,* Livermore, CA 94550

*To whom correspondence should be addressed. E-mail: martine.duff@srnl.doe.gov

Keywords: CdZnTe, transmission electron microscopy, scanning electron microscopy, radiation detection

ABSTRACT

CdZnTe or "CZT" crystals are highly suitable for use as a room temperature based spectrometer for the detection and characterization of gamma radiation. Over the last decade, the methods for growing high quality CZT have improved the quality of the produced crystals however there are material features that can influence the performance of these materials as radiation detectors. For example, various structural heterogeneities within the CZT crystals, such as twinning, pipes, grain boundaries (polycrystallinity), and secondary phases (SP) can have a negative impact on the detector performance. In this study, a CZT material was grown by the modified vertical Bridgman growth (MVB) method with zone leveled growth without excess Te in the melt. Visual observations of material from the growth of this material revealed significant voids and SP. Three samples from this material was analyzed using various analytical techniques to evaluate its electrical properties, purity and detector performance as radiation spectrometers and to determine the morphology, dimension and elemental /structural composition of one of the SP in this material. This material was found to have a high resistivity but poor radiation spectrometer performance. It had SP that were rich in polycrystalline aluminum oxide (Al_2O_3), metallic Te and polycrystalline CdZnTe and 15 to 50 μm in diameter. Bulk elemental analyses of sister material from elsewhere in the boule did not contain high levels of Al so there is considerable elemental impurity heterogeneity within the boule from this growth.

KEYWORDS: Modified vertical Bridgman, topography, TEM, aluminum, secondary phases

1. INTRODUCTION

CdZnTe (or CZT) crystals can be used in a variety of detector-type applications and it is a large band gap material that shows great promise for use as a gamma radiation spectrometer. The performance of CZT is been adversely affected by point defects, structural and compositional heterogeneities within the crystals, such as twinning, pipes, grain boundaries (polycrystallinity), various types of voids and SP.[1-6] However, as the size of useful detectors gradually increased from a few mm^3 to a few cm^3, the limiting factor in the detector performance seemed to vary from electron and hole trapping by point defects, pipes and cracks to what has more recently been named in the literature as either Te inclusions [as recently described by Carini et al. (2006), Bolotnikov et al. (2007) and refs. therein] or as Te precipitates.[6-8] One explanation for formation of Te-rich SP is has been attributed to excess Te in the melt of CZT and CdTe phases. Even if the starting charge is stoichiometric or slightly Cd-rich, elemental Cd, which is the most volatile elements in the melt will preferentially evaporate into the free space of the ampoule and leave behind a Te-rich melt. Such Te-rich phases may form during crystal growth or post growth annealing due to the retrograde solubility within the phase diagram.[9-10] Such SP were noted by Duff and researchers (2009) when they observed the less than 10% of the SP population in detector grade MVB grown CZT were 20 μm sized spherical (faceted) bodies that were rich in Te in addition to being rich in Cd and Zn.[11] Most all (90%) of the SP in this particular MVB grown material were triangular-shaped 20 μm sized voids with trace levels of nanoparticulate CdZnTe residues. These triangular-shaped voids and the somewhat spherical Te, Cd and Zn-rich SP were readily observed as being dark features in transmission IR imaging studies.

Improvements in the CZT growth methods have addressed the issue of the performance-limiting cracks and the voids within pipe features, which appear as dark features in transmission IR images. CZT crystals made using low pressure MVB[12] and the traveling heater method or THM (by Redlen Technologies in Canada)[13,14] growth processes provide good control of the growth and they produce large (seeded) single crystals. The synthesis of CZT has improved greatly during the last 15 years however the primary performance limitation of CZT for use as a radiation spectrometer is attributed to the presence of SP. In this presentation, we will describe the characterization of a CZT material with poor radiation detector performance with the use of IR imaging, electron microscopy, I-V curves, electron mobility and elemental compositional analyses.

2. EXPERIMENTAL

A small CZT crystal with the dimension of 1 x 1 x 0.2 cm^3 that we characterized in this study was grown at Washington State University using a zone leveled MVB growth method.[13-16] In this method, Cadmium Zinc Telluride (CdZnTe- with 10% Zn) is grown as a single crystal boule 47 mm in diameter and 118 mm long was produced. No Te excess was used in the melt and all metals used were >6N purity. The feed materials were doped with indium to compensate for electrical defects that are related to Cd loss during growth. Grown boules were cut to appropriate thickness to provide a final detector thickness of roughly 2 mm. The techniques that were used included measurements of electronic properties through mu tau electron mobility and detector performance tests with radiation sources. We also performed visible and transmission IR imaging. After polishing with alumina powders down to 0.3 μm, these crystals were characterized by transmission IR imaging using a Sony CCD-IRIS camera for image recording. They were then prepared with gold (Au) contacts deposited by sputtering in vacuum. The Au contacts allowed for detector performance testing in a planar geometry using ^{57}Co and ^{241}Am gamma sources using a Tennelec amplifier. Current-voltage (I-V) curves were obtained using the Keithley 237 Power Unit assisted by a PC computer using the ICS (Interactive Characterization Software) software of Metrics Technology Inc.

After the above characterization, this Au-sputtered material was sent to LLNL for examination by SEM using an FEI Nova 600 Nanolab Dualbeam Focussed Ion Beam Scanning Electron Microscope (FIB-SEM) at 5 keV to analyze and produce thin sections of SP-based areas of interest through focused ion-beam milling for high resolution-transmission electron microscopy (HR-TEM) studies. The HR-TEM studies were performed with a 200 keV FEI Technai20 G2 FEG monochromated scanning transmission electron microscope (STEM) with high angle annular dark field (HAADF) detector using a Si(Li) solid state X-ray detector with 0.3 steradians solid angle.

3. RESULTS AND DISCUSSION

Optical Images of a vertical slice of the boule and the location of the sample selected to be the focus of our study are shown in Fig. 1a and 1b. The elemental composition of samples taken near CG43.AC.C1 is shown in Table 1 (CG43.D.2), along with data showing the elemental compositions of two sister CG43.D.7 and CG43.D.9 samples from this growth. Samples CG43.D.2 was taken near C1 and C2, at the shoulder, D7 in the middle and D9 at the heel or last to freeze section of the ingot. Relative to the other two sister samples, the CG43.AC.1 contained a high level of Al, Mg, Cl, Fe and Cu. A photo of unpolarized IR light was used to examine for cracks, voids, grain boundaries and others

major defects in their volume. Secondary phases of unknown composition were readily viewed in a vertical slice of this material as shown in Fig. 2a. The electron mobility behavior (mu tau_e) of this CG43.AC.C2 sample is shown in Fig. 2b. I-V curve measurements revealed that the material has a high resistivity (Fig. 3a and b) of $\rho v = 5.85 \times 10^9$ Ωcm. The detector performance of this crystal was determined using the two radiation sources, shown in Fig. 4a and b. The Pulser FWHM values for CG43.AC.1 were 17.18% for a ^{57}Co gamma source and 16.52% for ^{241}Am gamma sources.

Scanning electron microscopy studies with CG43.AC.1 revealed the presence of SP of 15 to 50 μm in diameter that were slightly recessed from the CZT surface (Fig. 5a-d). The recessing may be due to the mechanical polishing, which may have removed more (physically labile) SP material than that of the single crystal CZT surface. Preparation of TEM thin sections from one of these SP using the FIB technique is shown in Fig. 6a-c. A low resolution TEM image of the thin section is shown in Fig. 6d and a higher resolution HAADF image of this section is shown in Fig. 7. Energy dispersive spectrometry (EDS) techniques (actual data now shown) during TEM analyses was used to determine the elemental composition of the SP within the thin section revealed considerable elemental composition heterogeneity as delineated in Fig. 7. Due to Au sputtering, Au was found in the crack between the SP and its host CZT material. Figure 8 reveals a close-up of a portion of the sample that was shown in Fig. 7. In this enlarged image (Fig. 8), regions of pure Te, single crystal CZT, polycrystalline CZT, and aluminum oxide (Al_2O_3) are intermixed within the SP material.

4. CONCLUSION

Although this material was of high resistivity, the presence of large voids, Al-rich SP, and high bulk Al likely had a negative influence on the radiation spectrometer performance of this material in our study. The SP in sample CG43.AC.1 were probably formed during growth because they served as reservoirs for trapping elemental impurities and localized excesses of Te within the host single crystal matrix. Whether these formed during crystal growth or cool-down could not be determined with the information presented in this paper. This presentation contributes new information about variety in then elemental composition and makeup of SP in CZT.

5. ACKNOWLEDGMENTS

This work was supported by the US DOE - National Nuclear Security Administration, through the Office of Nonproliferation Research and Development - NA-22.

6. REFERENCES

1. J.R. Heffelfinger, D.L. Medlin, and R.B. James. MRS Symp. Ser. 487, 33 (1998).

2. M. Schieber, T.E. Schlesinger, R.B. James, H. Hermon, H. Yoon, and M. Goorsky. J. Crystal Growth 237-239, 2082 (2002).

3. C. Szeles, and M.C. Driver. SPIE Proc. 3446, 1 (1998).

4. C. Szeles, S.E. Cameron, J-O. Ndap, and W.C. Chalmers. IEEE Trans. Nucl. Sci. 49, 2535 (2002).

5. J. Shen, D. K. Aidun, L. Regel, and W.R. Wilcox. J. Crystal Growth 132, 250 (1993).

6. G.A. Carini, A.E. Bolotnikov, G.S. Camarda, G.W. Wright, L. Li, and R.B. James. Appl. Phys. Lett. 88, 143515 (2006).

7. A.E. Bolotnikov, G.S. Camarda, G.A. Carini, Y. Cui, L. Li, and R.B. James, Nucl. Instrum. Meth. A571, 687 (2007).

8. C. Szeles, W.C. Chalmers, S.C. Cameron, J-O. Ndap, M. Bliss, and K.G. Lynn. SPIE Proc. 4507, 57 (2001).

9. P. Rudolph, M. Neubert, and M. Mühlberg. J. Crystal Growth 128, 582 (1993).

10. P. Rudolph, A. Engel, I. Schentke, and A. Grochochi. J. Crystal Growth 147, 297 (1995).

11. M.C. Duff, D.B. Hunter, A. Burger, M. Groza, V. Buliga, J.P. Bradley, G. Graham, Z. Dai, N. Teslich, D.R. Black, and A. Lanzirotti, J. Mat. Res. 24, 1361 (2009).

12. L. Li, F. Lu, K. Shah, M. Squillante, L. Cirinano, W. Yao, R.W. Olson, P. Luke, Y. Nemirovsky, A. Burger, G. Wright, and R.B. James. Nucl. Sci. Symp. Conf. Rec. IEEE 4, 2396 (2001).

13. H. Chen, S. A. Awadalla, J. Mackenzie, R. Redden, G. Bindley, A. E. Bolotnikov, G. S. Camarda, G. Carini, and R. B. James. IEEE Trans. Nucl. Sci., 54, 811 (2007).

14. H. Chen, S.A. Awadalla, K. Iniewski, P.H. Lu, F. Harris, J. Mackenzie, T. Hasanen, W. Chen, R. Redden, G. Bindley, I. Kuvvetli, C. Budtz-Jørgensen, P. Luke, M. Amman, J.S. Lee, A.E. Bolotnikov, G.S. Camarda**,** Y. Cui, A. Hossain, and R.B. James. J. Appl. Phys. 103, 014903 (2008).

Table 1. Glow Discharge Mass Spectrometric Report - ppb (atomic)

	CdZnTe CG43.D.2	CdZnTe CG43.D.7	CdZnTe CG43.D.9		CdZnTe CG43.D.2	CdZnTe CG43.D.7	CdZnTe CG43.D.9
Li	8	5	5	La	<0.6	<0.6	<0.3
Be	<2	<2	<2	Ce	<3	<2	<0.7
B	<5	<4	<4	Pr	-	-	-
C	1200	580	160	Nd	-	-	-
N	70	50	20	Sm	-	-	-
O	1100	540	200	Eu	-	-	-
H	-	-	-	Gd	-	-	-
F	<7	<7	<5	Tb	-	-	-
Na	89	130	240	Dy	-	-	-
Mg	17	15	36	Ho	-	-	-
Al	6	8	20	Er	-	-	-
Si	13	17	<2	Tm	-	-	-
P	17	<3	<2	Yb	-	-	-
S	81	54	26	Lu	-	-	-
Cl	98	12	<4	Hf	<4	<9	<10
K	<65	<90	<50	Ta	-	-	-
Ca	<50	<35	<25	W	<2	<2	<2
Sc	<0.6	<0.6	<0.5	Re	<1	<1	<0.9
Ti	<0.6	<0.6	<0.4	Os	<5	<6	<5
V	<0.3	<0.3	<0.2	Ir	<2	<2	<1
Cr	<4	<4	<2	Pt	<8	<11	<6
Mn	<10	<10	<10	Au	<5	<5	<5
Fe	83	54	56	Hg	<4	<4	<3
Co	<0.7	<0.6	<0.5	Tl	<2	<1	<0.8
Ni	<3	<3	<2	Pb	<2	<1	<0.8
Cu	24	<20	63	Bi	<0.7	<0.9	<0.7
Zn	(3.1%)	(3.6%)	(2.8%)	Th	<0.6	<0.6	<0.7
Ga	<6	<3	<3	U	<1	<1	<1
Ge	<20	<20	<20				
As	<15	<20	<15				
Se	<10	<10	<10				
Br	-	-	-				
Rb	<0.3	<0.4	<0.4				
Sr	<0.3	<0.3	<0.2				
Y	<0.2	<0.3	<0.2				
Zr	<0.6	<0.4	<0.3				
Nb	<0.8	<0.2	<0.2				
Mo	<2	<3	<1				
Ru	<6	<5	<6				
Rh	<30	<50	<25				
Pd	<35	<25	<30				
Ag	<50	<45	<85				
Cd	Matrix	Matrix	Matrix				
In	8800	1900	3300				
Sn	<20	<20	<20				
Sb	<40	<55	<40				
Te	Matrix	Matrix	Matrix				
I	<530	<910	<550				
Cs	<2	<2	<1				
Ba	<4	<3	<0.6				

a)

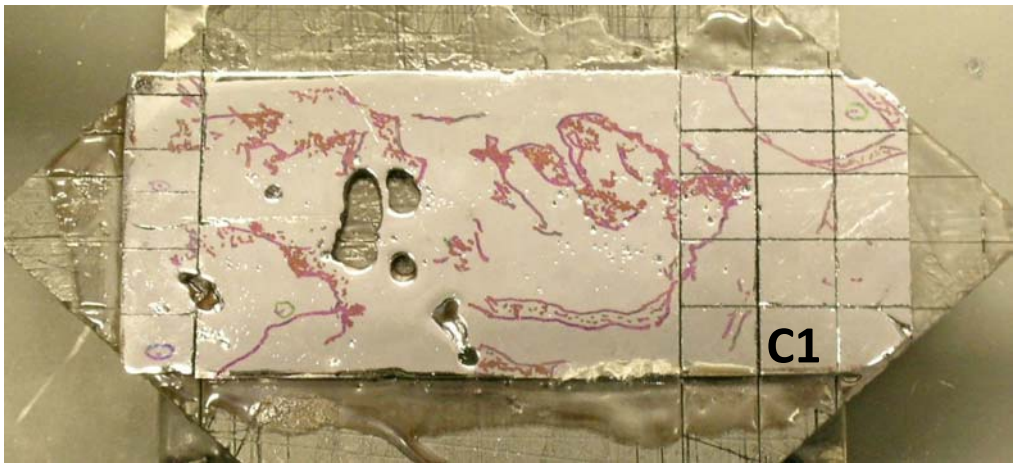

b)

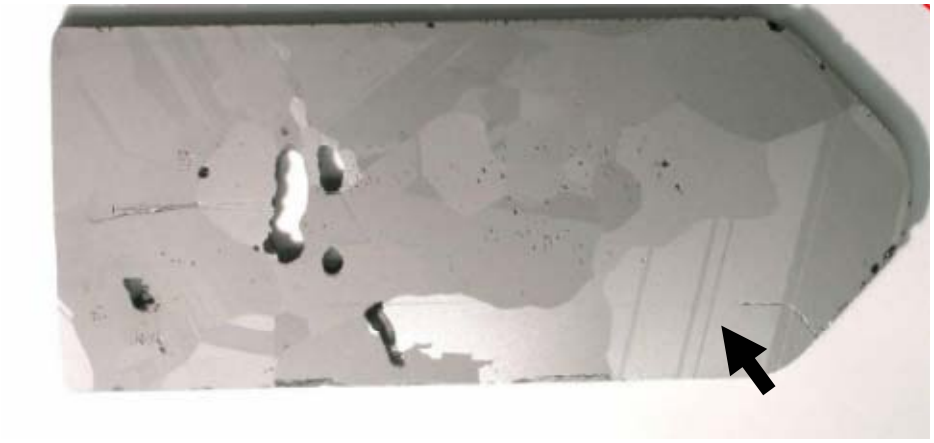

Fig. 1. Optical photographic images of a) a vertical slice of CG43 and the location of C1 with grain boundaries enhanced by red pen and b) another vertical slice without grain boundary enhancement-note the presence of twinning in lower right portion (see arrow).

a)

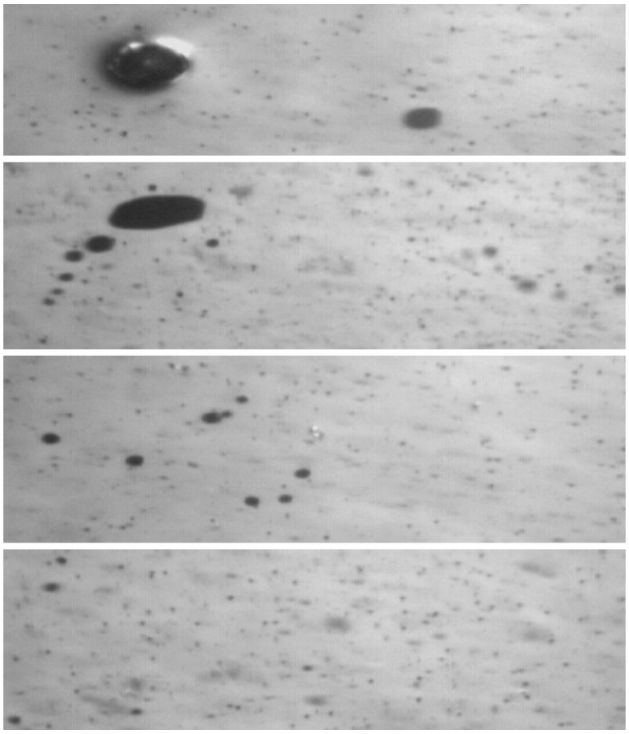

b)

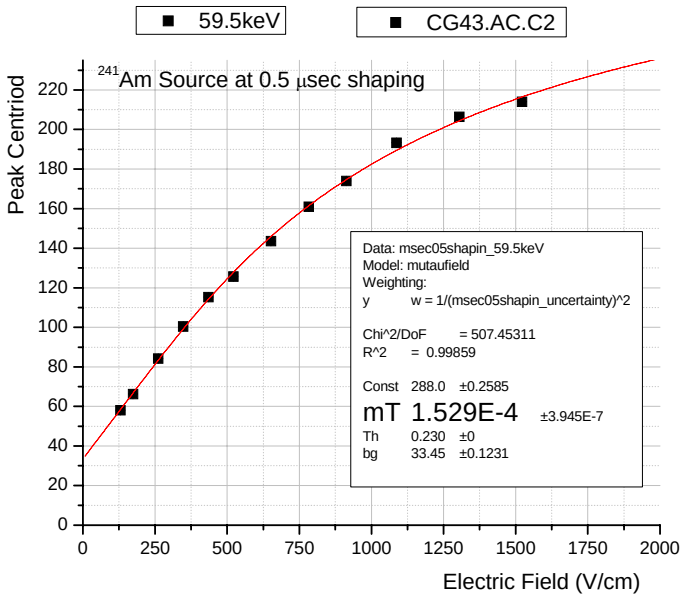

Fig. 2. a) Several transmission IR images taken at four different locations within sample CG43.AC.C1 and b) the electron mobility mu tau_e measurement data for CG43.AC.C1.

a)

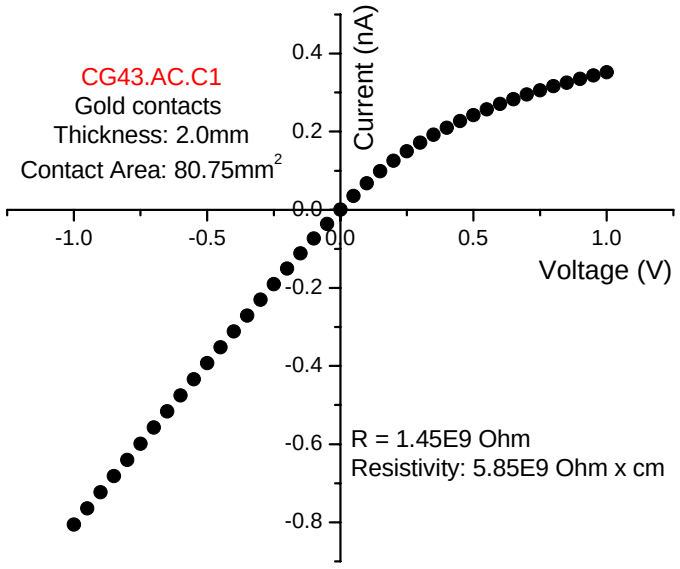

b)

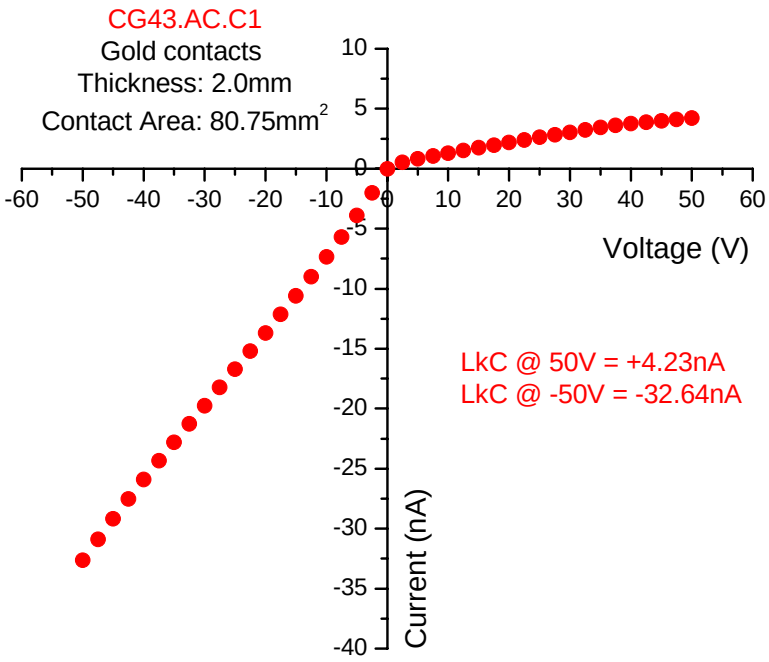

Fig. 3. I-V curve measurements for CG43.AC.C1 for voltages between a) -1.0 V and +1.0 V and b) -50V and +50V for the sample which had a high resistivity of 5.85 x 10^9 Ohm cm.

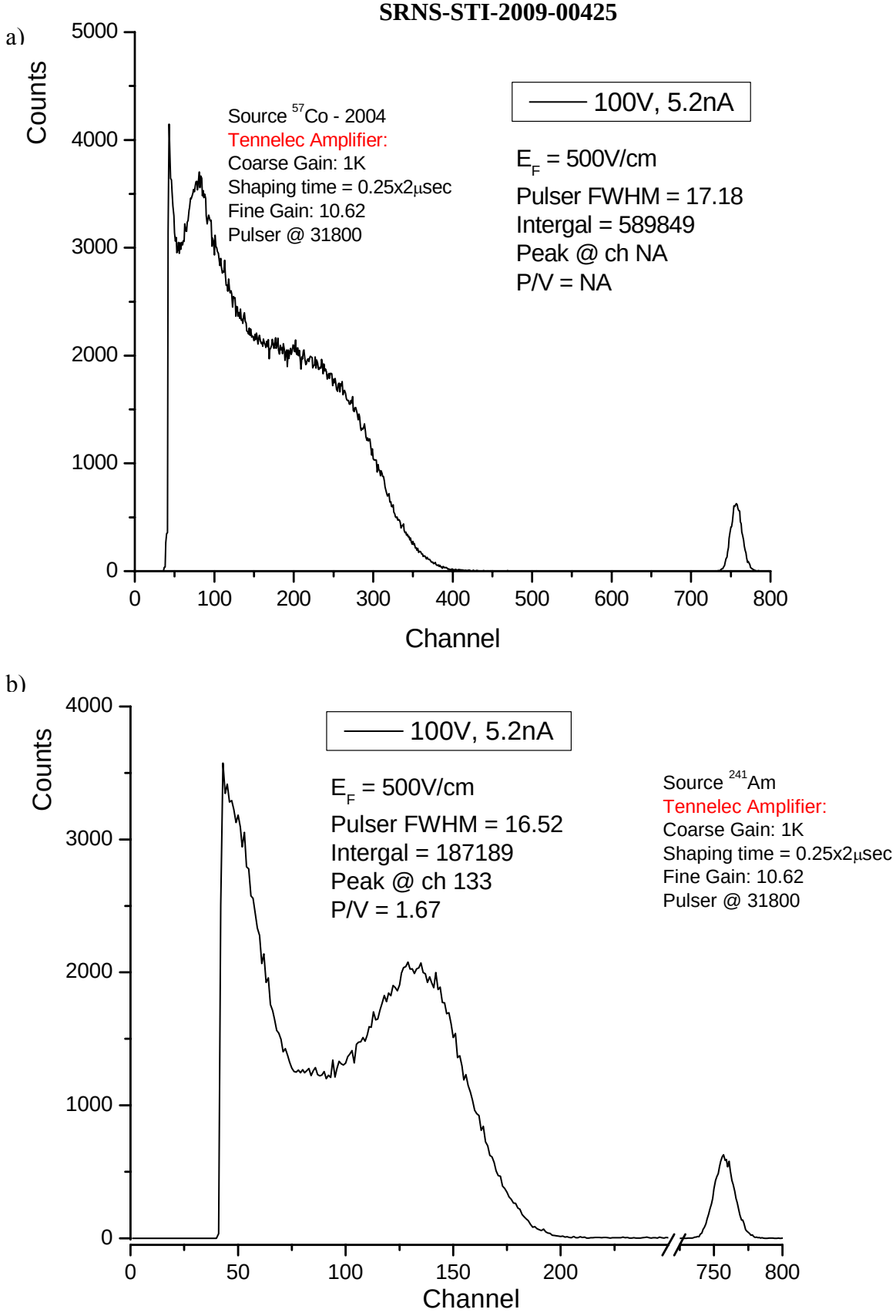

Fig. 4. Gamma radiation spectrometer performance studies with CG43.AC.C1 using a) ^{57}Co and b) ^{241}Am.

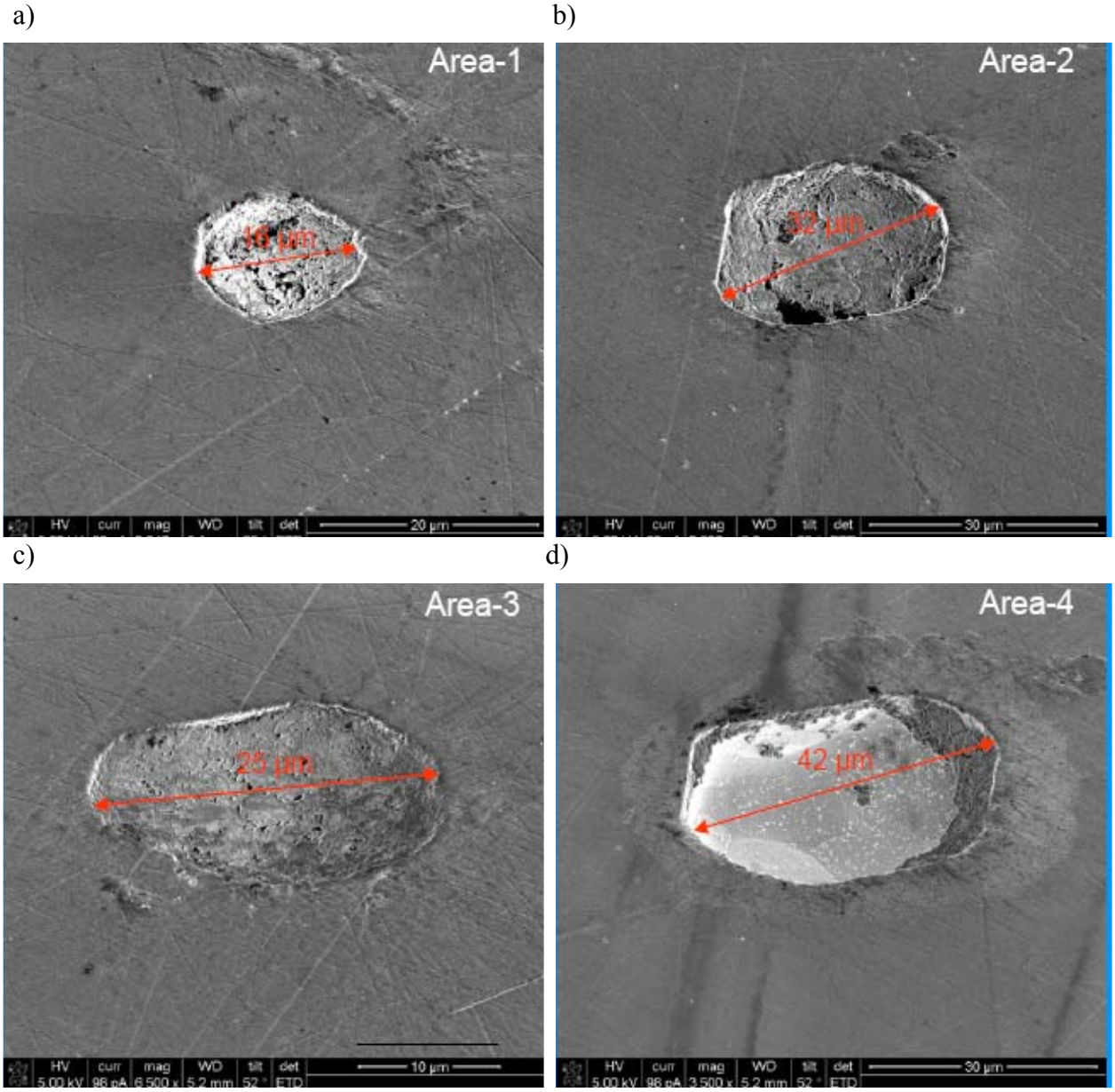

Fig. 5a-d. Scanning electron images of four SP on the surface of sample CG43.AC.C1.

a) b)

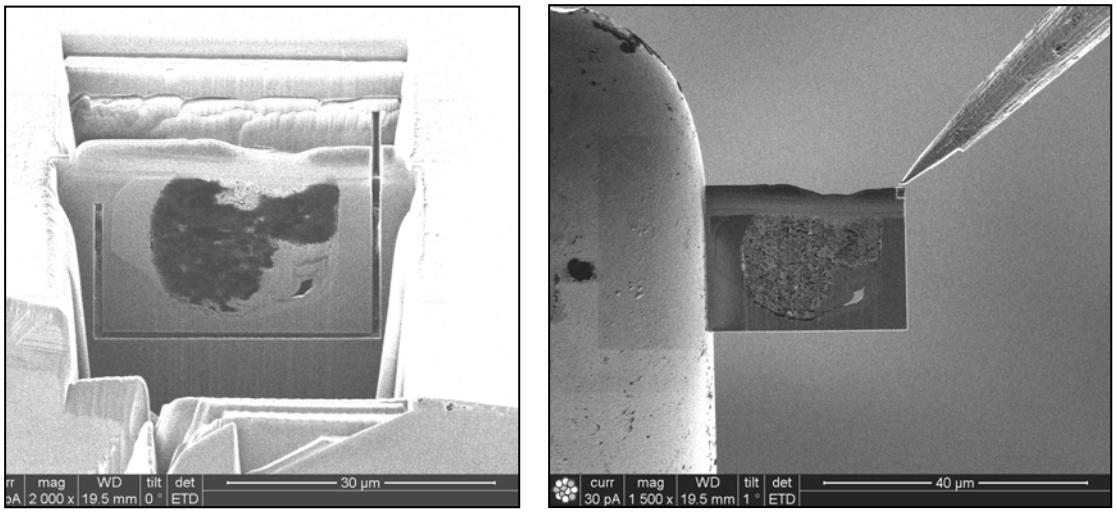

c) d)

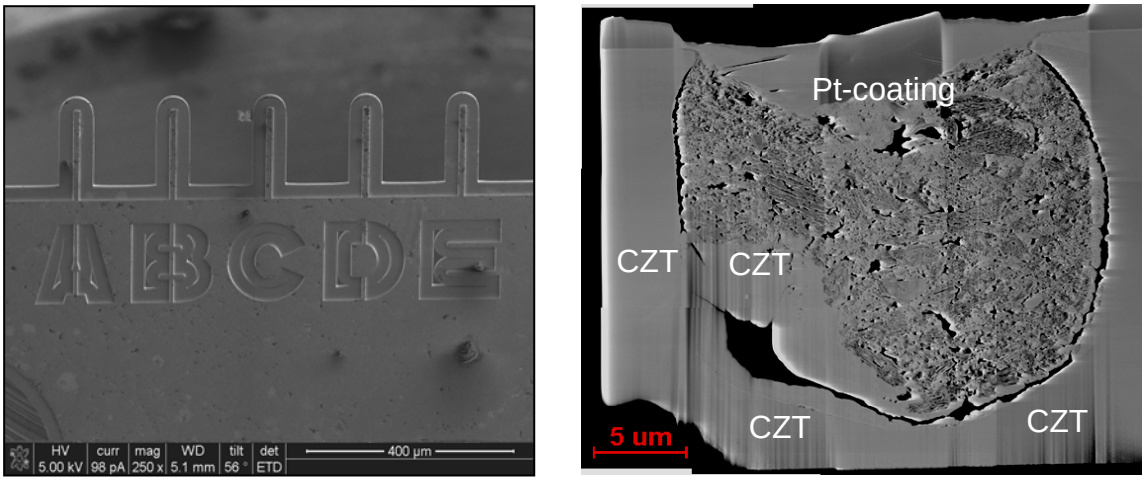

Fig. 6a-c. The process of using FIB milling to prepare a thin section for transmission electron microscopy and d) a low resolution TEM image of the SP in sample CG43.AC.C1.

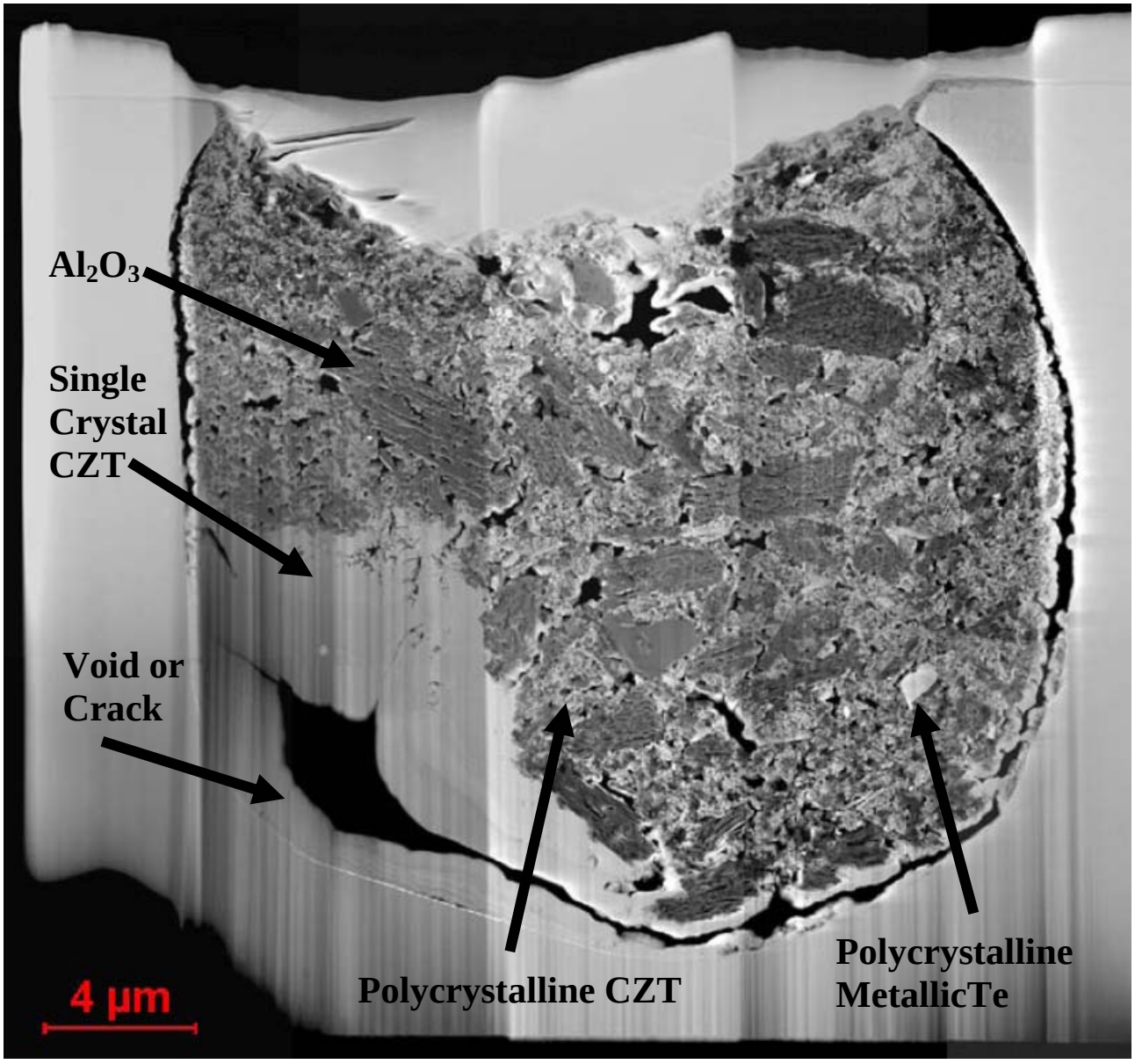

Fig. 7. High resolution image of the SP in CG43.AC.C1 using the high angle annular dark field (HAADF) technique.

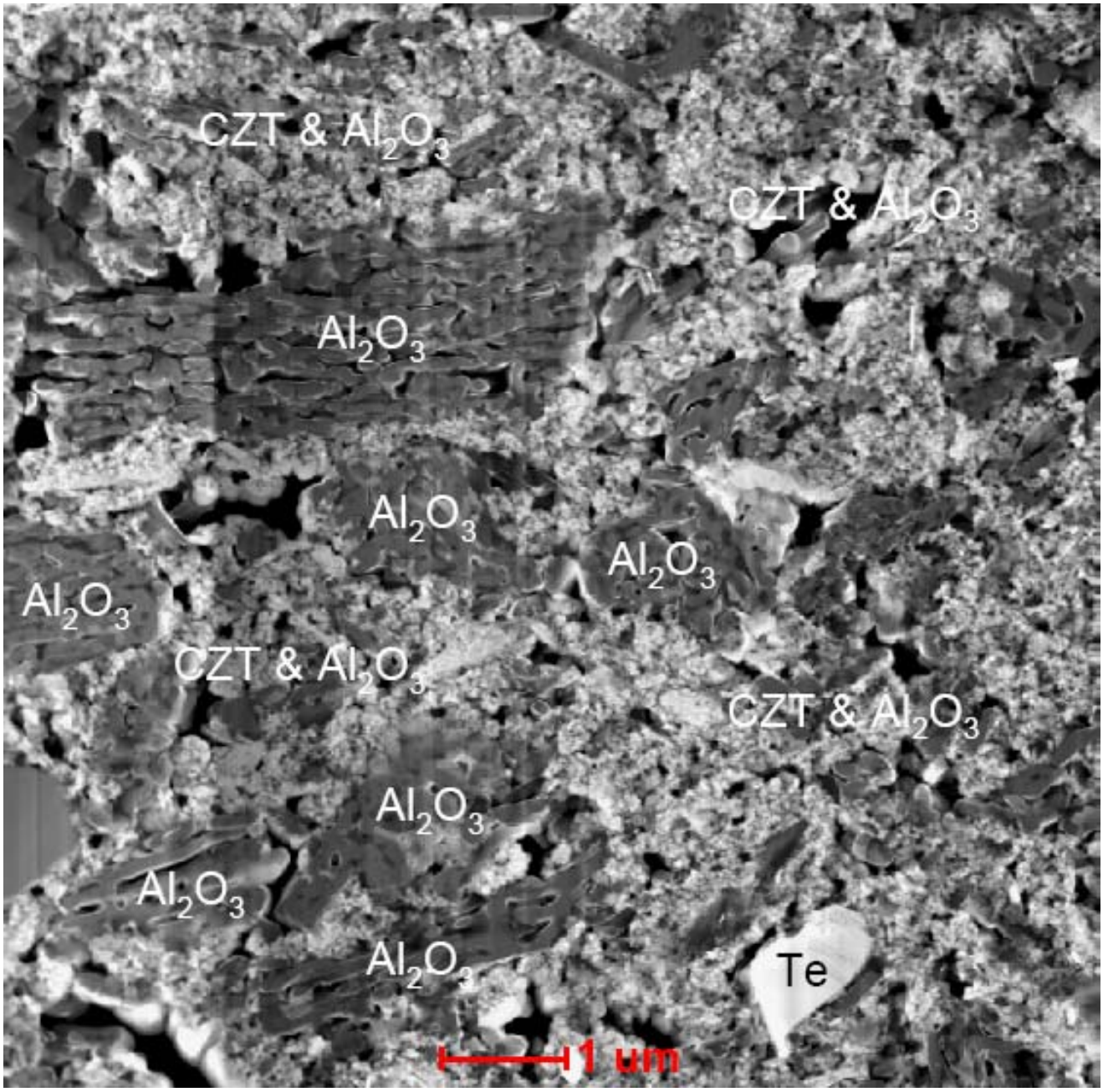

Fig. 8. HAADF imaging detail of features in SP within CG43.AC.C1.